Proceedings of the Project Review, Geo-Mathematical Imaging Group (Purdue University, West Lafayette IN), Vol. 1 (2008) pp. 129-139.

FOCUSED GAUSSIAN BEAMS FOR SEISMIC IMAGING

ROBERT L. NOWACK*

Abstract. The application of focused Gaussian beams is investigated for the seismic imaging of common-shot reflection data. The focusing of Gaussian beams away from the source and receiver surface adds flexibility to beam imaging algorithms allowing for the narrowest portions of the beams to occur at the depth of a specific target structure. This minimizes the number of beams required to form an image at the target depth. The beam fronts at the beam-waists are also planar leading to more stable beam summations for imaging. To match with the surface data, a quadratic phase correction is required for the local slant-stacks of the data. Also, to use the same local slant stacks of the data for the different imaging depths, only a single focusing depth can be specified. Imaging using focused Gaussian beams is tested using a single shot gather for a model with 5 scatterers at different depths. The approach is then tested for a single shot gather from the Sigsbee2A model. In all cases, the beams can be focused to a particular target depth, but proper imaging still results for other depths as well.

1. Introduction. Seismic migration using focused Gaussian beams is applied for the inversion of common-shot reflection data. Focused Gaussian beams provide an added level of controllability of the individual beam solutions. It allows for the beam-waist to be placed at some depth away from the source and receiver surface and requires fewer beams for the imaging of a target structure at depth. In addition, beam fronts are planar at the beam-waists which provide more stable imaging. However, using focused beams results in generally curved beam fronts along the source and receiver aperture. In order to match initially curved beam fronts with the data, a quadratic phase correction term is needed for the local stacks of the data. In addition, for fixed spatial windows of the data, the windowing of the data can be related to the beam parameters of the propagated beams.

Summations of Gaussian beams over either initial take-off angle or position along an initial surface have been applied for the computation of high frequency seismic wavefields in smoothly varying inhomogeneous media (see for example, Popov, 1982; Cerveny et al. 1982; Nowack and Aki, 1984). Reviews of Gaussian beam summation have been given by Cerveny (1985a,b), Babich and Popov (1989), and more recently by Popov (2002), Nowack (2003), Cerveny et al. (2007) and Bleistein (2007). An advantage of summations using Gaussian beams to construct more general wavefields is that the individual Gaussian beams have no singularities along their paths, no two-point ray tracing is required and triplicated arrivals are naturally incorporated into either forward or inverse modeling. More recently over-complete frame-based Gaussian beam summations have been developed based on window and wavelet transforms to address some of the issues related to completeness of beam summations (Lugara et al., 2003). In an over-complete frame based approach, the wavefield is decomposed into beam fields that are localized both in position and direction. Although an orthonormal basis cannot be formed using a Gabor frame, an over-complete frame expansion can be constructed which has the added benefit of providing redundancy in the expansion (Feichtinger and Strohmer, 1998; Hill; 1990, 2001; Hale, 1992). Here curved initial beams are used to decompose the data and these are then propagated into the subsurface using focused Gaussian beams.

In order to test the focused Gaussian beam approach, a test model is constructed with 5 small scatterers with depth in a vertically varying medium resulting in 5 diffracted arrivals each with different move-outs with distance. The partial images of single beams with different focusing depths are shown with narrow and planar images of the scatterers for each focusing depth. However, when summed over angles and data windows, all the scatterers are properly imaged no matter what specific focusing depth is used. Focused Gaussian beam migration is then tested on a portion of the Sigsbee2a model, away from the salt body, and correct imaging occurs for all depths for the different beam focusing parameters. The advantage of using focused beams for a target structure at a specific depth is that fewer beams are required for that image depth.

*Dept. of Earth and Atmos. Sci., Purdue University, West Lafayette, IN 47907, USA (nowack@purdue.edu).

2. Overview of Gaussian Beam Imaging with Focusing Beams. In common-shot migration, each shot gather is migrated separately and the results are summed to give the final image. Thus,

$$\delta m(\underline{x}) \sim \int d\underline{x}^s I^s(\underline{x}) \ , \tag{2.1}$$

where the adjoint image for each shot point can be written

$$I^s(\underline{x}) = \int \frac{d\omega}{2\pi} K(\omega) \int d\underline{x}^g \overline{g}(\underline{x}, \underline{x}^s, \omega) \overline{g}(\underline{x}, \underline{x}^g, \omega) u_s(\underline{x}^g, \underline{x}^s, \omega) \ , \tag{2.2}$$

and

$$K(\omega) = \omega^2 \bar{S}(\omega) \ . \tag{2.3}$$

From reciprocity of the Green's function $g(x, x^{'}, \omega) = g(x^{'}, x, \omega)$ and $\overline{g}$ indicates the complex conjugate of g.

In the 2-D case, the Green's function can be written in terms of a summation of Gaussian beams as

$$g(\underline{x}, \underline{x}', \omega) = \frac{-\mathrm{i}}{4\pi} \left(\frac{\varepsilon}{v_0} \right)^{1/2} \int d\gamma u_\gamma^{\mathrm{gb}}(\underline{x}, \underline{x}', \omega) = \frac{-\mathrm{i}}{4\pi} \left(\frac{\varepsilon}{v_0} \right)^{1/2} \int \frac{\mathrm{dp}_1^r}{p_3^r} u^{\mathrm{gb}}(\underline{x}, \underline{x}', \underline{p^r}, \omega) \tag{2.4}$$

where ε is the beam parameter in Eqn. (7c) (Cerveny et al., 1982), and

$$u_\gamma^{\mathrm{gb}}(\underline{x}, \underline{x}', \omega) = \left[\frac{v(s)}{q(s)} \right]^{1/2} \exp \left\{ \mathrm{i}\omega\tau(s) + \frac{\mathrm{i}\omega}{2} M(s) n^2 \right\} \tag{2.5}$$

The coordinates (s,n) correspond to the position $\underline{x}$ in ray centered coordinates, $\tau(s)$ is the travel-time along the central ray, $v(s)$ is the velocity along the central ray and the horizontal component of the ray parameter vector at the source is $p_1^r = \sin\gamma / v_0$.

The complex second derivative of the travel-time field with respect to the transverse coordinate n can be written

$$M(s) = M_R(s) + \mathrm{i} M_I(s) = p(s)/q(s) \tag{2.6}$$

where $M_R(s)$ is related to the wavefront curvature $K(s)$ of the beam by $M_R(s) = K(s)/v(s)$. To form a bounded beam, then $M_I(s) > 0$. The variables $p(s)$ and $q(s)$ are solutions to the dynamic ray equations and for a beam solution are also complex (Cerveny, 2000). The dynamic ray equations in 2D have two real fundamental solutions which can be written as

$$\pi(s) = \begin{bmatrix} q_1(s) & q_2(s) \\ p_1(s) & p_2(s) \end{bmatrix} \tag{2.7}$$

where $\pi(s_0) = I$, $q_1(s)$, and $p_1(s)$ are solutions for an initial plane wave and $q_2(s)$ and $p_2(s)$ are for an initial point source. The two real solutions of the dynamic ray equations are then blended to form a beam. There are a number of ways to combine the solutions, but one way is (Cerveny et al., 1982)

$$q(s) = \varepsilon q_1(s) + q_2(s) \tag{2.8}$$

and

$$p(s) = \varepsilon p_1(s) + p_2(s) \tag{2.9}$$

where ε is the beam parameter. The variable $q(s)$ is related to the complex geometrical spreading along the beam. Since for the fundamental solution matrix $Det(\pi(s)) = 1$ for all points along the ray, the complex geometric spreading can never be zero at any point along the beam if it is non-zero at any one point. Since the beam amplitude is related to the inverse square root of the geometric spreading, the beam amplitudes are always finite, even at caustics for the ray solution. This is one of the useful features of beam solutions in contrast to ray solutions.

The second derivative of the time field with respect to n can be written as

$$M(s) = M_R(s) + \mathrm{i}M_I(s) = \frac{\varepsilon p_1(s) + p_2(s)}{\varepsilon q_1(s) + q_2(s)} \tag{2.10}$$

Since at the source point $\pi(s_0) = 1$ and $\varepsilon = \varepsilon_R - \mathrm{i}\varepsilon_I$, then

$$M(s_{_0}) = M_R(s_0) + \mathrm{i}M_I(s_0) = \frac{1}{\varepsilon} = \frac{\varepsilon_R}{\varepsilon * \varepsilon} + \frac{\mathrm{i}\varepsilon_I}{\varepsilon * \varepsilon} \tag{2.11}$$

where $\varepsilon * \varepsilon$ is the magnitude squared of ε. Alternatively, ε can be written in terms of $M(s_0)$ as

$$\varepsilon = \frac{M_R(s_0)}{M(s_{_0}) * M(s_{_0})} - \frac{\mathrm{i}M_I(s_0)}{M(s_{_0}) * M(s_{_0})} \tag{2.12}$$

where $M(s_0) * M(s_0)$ is the magnitude squared of $M(s_0)$. Thus, the complex beam parameter can be specified either directly in terms of ε or in terms of $M(s_0)$.

The complex beam parameter can also be written

$$\varepsilon = \varepsilon_r - \mathrm{i}\varepsilon_i = v_0 S_0 - \mathrm{i}v_0 L_0^2 \tag{2.13}$$

where v_0 is an initial velocity. In a homogeneous medium, S_0 is the distance of the beam waist from the initial point of beam. The exponential term away from the central ray can be written as

$$\exp\left\{\frac{-\omega}{2} M_I(s) n^2\right\} = \exp\left\{\frac{-n^2}{2L^2(s)}\right\} \tag{2.14}$$

where $L(s) = (\omega M_I(s))^{-1/2}$ is the beam half-width transverse to the ray. At the initial point of the beam, $L(s_0) = (\omega M_I(s_0))^{-1/2} = (\frac{\varepsilon * \varepsilon}{\omega \varepsilon_I})^{1/2}$. For the case when $S_0 = 0$, then the beam-waist is at the initial point of the beam with $M_R(s_0) = 0$, and $L(s_0) = (\frac{v_0}{\omega})^{1/2} L_0$ is the beam half-width at the beam-waist. In a homogeneous medium, this is the narrowest point along the beam and is also the only point where the beam front is planar. For the case when $S_0 \neq 0$, the beam front is curved at the initial position $s = s_0$ and the beam-waist is shifted along the beam away from the initial point of the beam. In a homogeneous medium, the planar beam-waist is at $s = S_0 - s_0$.

Although the planar beam-waist is often placed at the initial source point, it is also common to put the beam-waist at the receiver location (Cerveny, 1985a,b). This reduces the number of beams required for the summation at the receiver, and also planar beam fronts at the receiver provide more

stable beam summations. The beam-waist can also be placed at other positions along the beam, for example at a sub-surface scattering point. Recent true amplitude migration formulations using Gaussian beams have used beams traced from the scattering points up to the surface with the beam-waists specified at the scattering points (Protasov and Cheverda, 2005; 2006). However, it is more economical to launch beams from the source and receiver positions down into the subsurface since there are fewer source and receiver locations than subsurface scattering points, and this minimizes the amount of beam tracing required. In order to locate the beam-waists in the subsurface when the beams are launched from the source and receiver aperture, then generally curved beam fronts are required along the source and receiver aperture.

For nonplanar beams at the source or receiver positions launched at some angle to the aperture plane, the quadratic part of the initial beam with respect to the horizontal x coordinate can be written

$$\exp\left\{\frac{-\omega}{2}\frac{K_x(s_0)}{v_0}(x-x_L)^2\right\}\exp\left\{\frac{-(x-x_L)^2}{2L^2_{x-\mathrm{ref}}(s)}\right\} \tag{2.15}$$

where $K_x(s_0)$ is the initial horizontal beam curvature, and $L_{x-\mathrm{ref}}(s_0)$ is the initial horizontal beam half-width at the reference frequency ω_{ref}. To match this with the initial parameters of the beam propagated into the medium, then the transverse coordinate of the beam $n = \cos\gamma(x - x_L)$ where γ is the angle of the beam with respect to the vertical. Given the initial values $K_x(s_0)$ and $L_{x-\mathrm{ref}}(s_0)$ along the source and receiver aperture, then the initial values for $M_R(s_0)$ and $M_I(s_0)$ for the beams are

$$M_R(s_0) = \frac{K_x(s_0)}{v_0\cos^2(\gamma)} \tag{2.16}$$

and

$$M_I(s_0) = (\omega_{\mathrm{ref}}\cos^2(\gamma)L^2_{x-\mathrm{ref}}(s_0))^{-1} \tag{2.17}$$

and from Eqn. (2.12), the initial beam parameter $\varepsilon = \varepsilon_r - \mathrm{i}\varepsilon_i$ can be obtained and used to construct the beam solution propagated into the medium.

The 2-D resolution of unity by Gaussian functions in the aperture plane is

$$1 \sim \frac{1}{\sqrt{2\pi}}\frac{\Delta L}{\sigma}\sum_{m=-\infty}^{\infty}\mathrm{e}^{-(x-m\Delta L)^2/2\sigma^2} \tag{2.18}$$

where

$$\Delta L \ll 2\sigma\ . \tag{2.19}$$

Assuming a regularly spaced set of beam centers $x_L = m\Delta L$ along the receiver array, the source locations of the Green's functions at the receivers can be phase shifted to these beam center locations with a phase adjustment of $p_1^g(x_1^g - m\Delta L) + \frac{K_x(s_0)(x_1^g - m\Delta L)^2}{2v_0}$. Then,

$$g(\underline{x},\underline{x}^g,\omega) \sim C^g\int\frac{\mathrm{d}p_1^g}{p_3^g}u^{\mathrm{gb}}(\underline{x},\underline{x}^L,\underline{p}^g,\omega)\mathrm{e}^{\mathrm{i}\omega(p_1^g(x_1^g-m\Delta L)+\frac{K_x(s_0)(x_1^g-m\Delta L)^2}{2v_0})}\ , \tag{2.20}$$

where C^g is the coefficient for the receiver Green's functions from Eqn. (2.4) and p_1^g is the horizontal component of the ray parameter vector along the receiver aperture. Eqn. (2.2) can then be written

$$I_s(\underline{x}) = \sum_{m=-\infty}^{\infty} \int \frac{d\omega}{2\pi} A_1(\omega) \int d\underline{x}^g \int \frac{\mathrm{dp}_1^g}{p_3^g} \bar{u}^{\mathrm{gb}}(\underline{x}, \underline{x}^L, \underline{p}^g, \omega) \mathrm{e}^{-\mathrm{i}\omega(p_1^g(x_1^g - m\Delta L) + \frac{K_x(s_0)(x_1^g - m\Delta L)^2}{2v_0})} \bar{g}(\underline{x}, \underline{x}^s, \omega) u_s(\underline{x}^r, \underline{x}^s, \omega) \mathrm{e}^{-(x_1^g - m\Delta L)^2/2\sigma^2} \tag{2.21}$$

where

$$A_1(\omega) = \left(\frac{+\mathrm{i}}{2\pi}\right) \left(\frac{\bar{\varepsilon}}{v_0^g}\right)^{1/2} \omega^2 \bar{S}(\omega) \frac{1}{\sqrt{2\pi}} \frac{\Delta L}{\sigma} \ . \tag{2.22}$$

The source Green's function now needs to be decomposed into Gaussian beams, but for simplicity here will be just referred to as $\bar{g}(\underline{x}, \underline{x}^s, \omega)$, where the over-bar signifies the complex conjugate.

The common-shot imaging formula for non-planar, focused beams along the aperture plane can then be written

$$I_s(\underline{x}) = \sum_{m=-\infty}^{\infty} \int \frac{d\omega}{2\pi} \int \frac{\mathrm{dp}_1^g}{p_3^g} A_1(\omega) \bar{g}(\underline{x}, \underline{x}^s, \omega) \bar{u}^{\mathrm{gb}}(\underline{x}, \underline{x}^L, \underline{p}^g, \omega) D_p(\underline{x}^L, \underline{x}^s, \underline{p}^g, \omega) \tag{2.23}$$

where

$$D_p(\underline{x}^L, \underline{x}^s, \underline{p}^g, \omega) = \int \mathrm{dx}_1^g u_s(\underline{x}^g, \underline{x}^s, \omega) \mathrm{e}^{-(x_1^g - m\Delta L)^2/2\sigma^2} \mathrm{e}^{-\mathrm{i}\omega(p_1^g(x_1^g - m\Delta L) + \frac{K_x(s_0)(x_1^g - m\Delta L)^2}{2v_0})} \tag{2.24}$$

This is a local slant-stack of the data with a quadratic phase correction term to match the data with the beams launched into the medium. The standard Gaussian beam migration formulas with the planar beam waists along the aperture plane does not include this quadratic phase correction term (Hill, 1990; 2001; Hale, 1992). The beam centers are spaced along the receiver aperture plane at

$$x_1^L = m\Delta L, \qquad \Delta L \ll 2\sigma \ . \tag{2.25}$$

and the initial horizontal beam widths are

$$\sigma = L_{x-\mathrm{ref}}(s_0) \left(\frac{\omega_r}{\omega}\right)^{1/2} \tag{2.26}$$

where $L_{x-\mathrm{ref}}(s_0)$ is the horizontal half-width of an initial Gaussian function at the reference frequency ω_{ref}. The spacing of the beams in horizontal position and launch angle can then be determined based either on physical reasoning (Hill, 1990; 2001; Hale, 1992), or by arguments based on frames (Feichtinger and Strohmer, 1998).

3. Applications of Focusing Gaussian beam Migration. In order to test the focusing beam migration formulation, two examples are given. The first application has 5 compact sources located at depths of 8,000, 12,000, 16,000, 20,000 and 24,0000 ft at a distance of 40,000 ft from the left side of the model. The background velocity model has two layers. The first layer has a thickness of 6000 ft with a constant velocity of 5000 ft/sec. The second layer goes from 6000 ft to 30,000 ft in depth with a vertical velocity gradient of $v(z) = v_0 + k(z - z_b)$ where $v_0 = 5000$ ft/sec, and $k = .15$. The shot position is located along the surface at a horizontal position of 40,000 ft from the left side of the model. The receiver array is from 25,000 ft to 55,000 ft on the surface. Figure

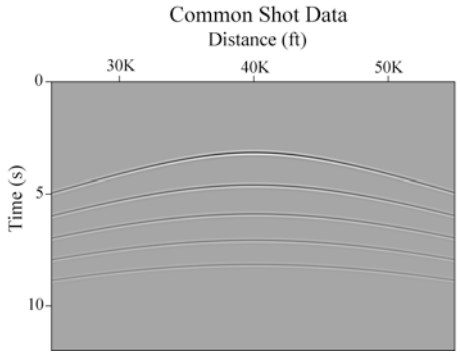

FIG. 1. *Computed common-shot data is shown for a shot point on the surface at a position of 40,000 ft. The receiver array is from 25,000 ft to 55,000 ft. Diffractions from 5 compact scatterers are shown each with a horizontal position of 40,000 ft and depths of 8,000, 12,000, 16,000, 20,000 and 24,000 ft.*

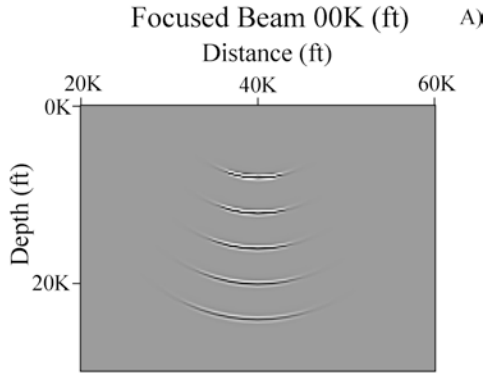

FIG. 2. *The partial image of the common shot data in Figure 1 using a single vertical Gaussian beam at a receiver position at 40,000 ft using a beam with a planar beam-waist at the surface.*

1 shows the computed wavefield from the 5 compact scatterers. The sampling rate is .008 sec and the peak frequency of the data is 5 Hz.

Figure 2 shows the partial image of the data from a single vertically propagated Gaussian beam with the planar wavefront at the surface. For simplicity the source side Green's function is constructed separately using Gaussian beams that are planar at the source location for all the examples given. Note on the figure that the images of the diffractors are curved and increase in width with depth. Figure 3 shows the partial image of the common shot data in Figure 1 using a single vertical Gaussian beam at a receiver position at 40,000 ft using a focused beam with the beam-waist at a depth of 12,000 ft. Now the diffractor at a depth of 12,000 ft is the most focused using a single beam with the images of the other diffractors being broader and generally curved. Figure 4 shows the partial image of the common shot data in Figure 1 using a single vertical Gaussian beam at a receiver position at 40,000 ft using a focused beam with the beam-waist at a depth of 16,000 ft. Now the diffractor at a depth of 16,000 ft is the most focused using a single beam with the images of the other diffractors being broader and curved. Figure 5 shows the partial image of the common shot data in Figure 1 using a single vertical Gaussian beam at a receiver position at 40,000 ft with a focused beam with the beam-waist at a depth of 20,000 ft. Now the diffractor at a depth of 20,000 ft is the most focused using a single beam with the images of the other diffractors being broader and curved. Finally, Figure 6 shows the partial image of the common shot data in Figure 1 using a single vertical Gaussian beam at a receiver position at 40,000 ft with a focused beam with the beam-waist at a depth of 24,000 ft. Now the diffractor at a depth of 24,000 ft is most the focused

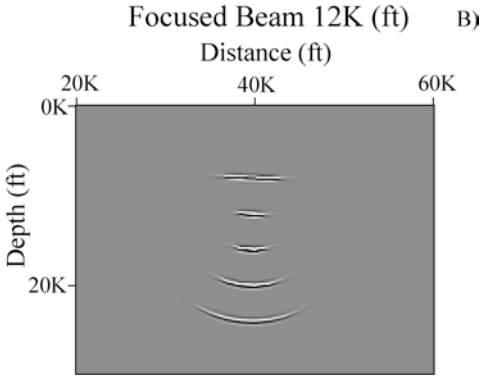

FIG. 3. *The partial image of the common shot data in Figure 1 using a single vertical Gaussian beam at a receiver position at 40,000 ft using a focused beam with a beam-waist at a depth of about 12,000 ft.*

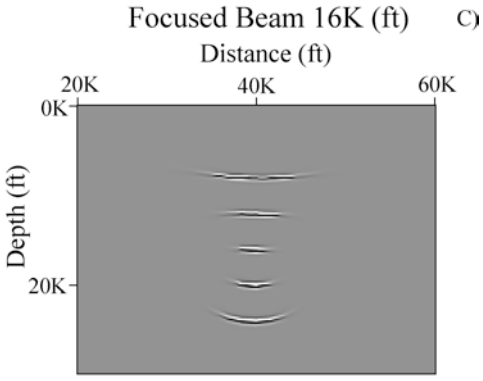

FIG. 4. *The partial image of the common shot data in Figure 1 using a single vertical Gaussian beam at a receiver position at 40,000 ft using a focused beam with a beam-waist at a depth of about 16,000 ft.*

using a single beam with the images of the other diffractors being broader and generally curved.

Figure 7 shows the partial image of the common shot data in Figure 1 using receiver beams centered on 40,000 ft now launched at all angles, each with the beam-waist shifted approximately 16,000 ft. This results in spherical images of all 5 scatterers and indicates that the imaging is being properly applied even with curved and broadened beams at the other depths. Using focusing beams with other beam-waist locations gives similar imaging results.

Figure 8 shows the complete Gaussian beam image for the single shot gather from Figure 1 using beams from all beam center locations launched at all angles, each with the beam-waist shifted approximately 16,000 ft. This results in focused images of all 5 scatterers and indicates that the imaging is being properly applied even with the shifted beam-waists of the individual beam components. Using focusing beams with other beam-waist locations gives similar imaging results.

The focusing beam migration approach is now applied to a single shot gather from the Sigsbee2A data set distributed by SMAART (Subsalt Multiples Attenuation and Reduction Team) and available at http://www.delphi.tudelft.nl/SMAART/ . In order to test the focused beam approach, a single shot gather with a shot location at 6,325 ft from the left edge of the model is used. The receiver array starts at the shot location and has a maximum offset of 26,025 ft with a spacing of 75 ft. The background velocity model has the first layer from the surface down to the seafloor with a velocity of 5000 ft/sec. The second layer goes from seafloor to 30,000 ft in depth with a background velocity of $v(z) = v_0 + k(z - z_{\text{seafloor}})$ where $v_0 = 5000$ ft/sec, and $k = .30$. A salt dome exists with

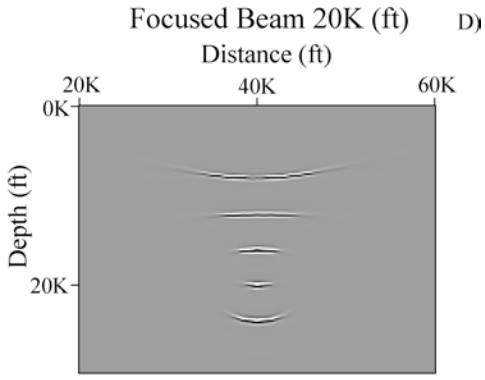

FIG. 5. *The partial image of the common shot data in Figure 1 using a single vertical Gaussian beam at a receiver position at 40,000 ft using a focused beam with a beam-waist at a depth of about 20,000 ft.*

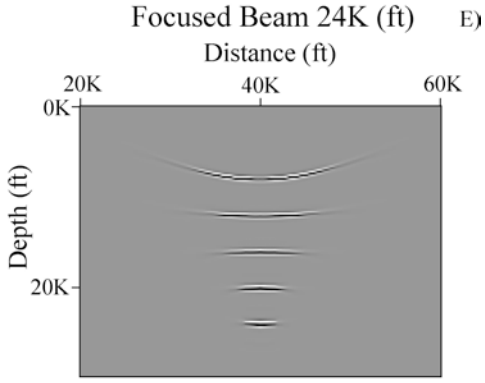

FIG. 6. *The partial image of the common shot data in Figure 1 using a single vertical Gaussian beam at a receiver position at 40,000 ft using a focused beam with a beam-waist at a depth of about 24,000 ft.*

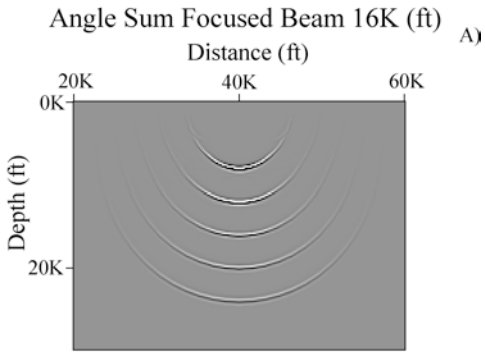

FIG. 7. *The partial image of the common shot data in Figure 1 using receiver beams centered on 40,000 ft now launched at all angles, each with the beam-waist shifted approximately 16,000 ft. This results in spherical images of all 5 scatterers and indicates that the imaging is being properly applied even with the shifted beam-waists of the individual beam components.*

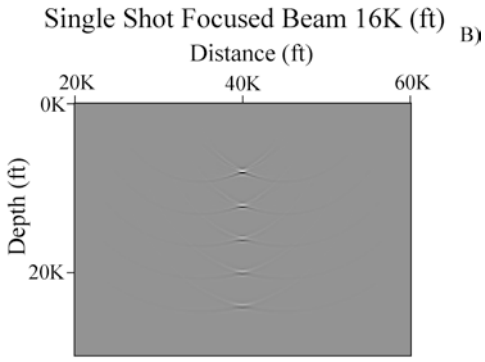

FIG. 8. *The Gaussian beam image using the complete single shot gather is shown in Figure 1 with beams from all beam positions launched at all angles, each with the beam-waist shifted to approximately 16,000 ft. This results in focused images of all 5 scatterers and indicates that the imaging is being properly applied even with the shifted beam-waists of the individual beam components.*

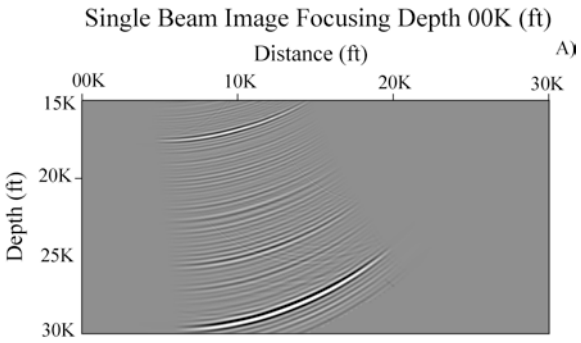

FIG. 9. *This shows the partial imaging result for a single Gaussian beam with the beam-waist at the surface along the receiver array for a single shot gather from the Sigsbee2A dataset.*

a velocity of *14,800 ft/sec* in the middle and right parts of the model, but for the initial tests here only a shot gather away from the salt dome is used.

In Figure 9, the partial imaging for a single Gaussian beam is shown with the planar beam-waist at the receiver depth. As in the earlier examples the source side Green's function is constructed separately using Gaussian beams that are planar at the source location. The receiver Gaussian beam has an initial location near the source and the partial image for a beam with a slight angle from the vertical is shown. As in the earlier example, when the beam-waist is at the receiver depth, then curved beam fronts result which broaden with depth over the depth range of the model shown between 15,000 and 30,000 ft. This is typical of standard implementations of Gaussian beam migration. However, in regions of a complicated background medium, the medium itself can cause additional focusing of the beams. This will be investigated later, but for this study only beam focusing resulting from the shifting of the beam-waists in the linear velocity gradient background velocity model is investigated.

Figure 10 shows the partial imaging results for a single Gaussian beam with the beam-waist shifted to about 20,000 ft in depth. At this depth the narrowest part of the beam image occurs and also with a planar beam front. If the target structure were located at this depth, then fewer beams would be required to form a complete image. Also the beam images would have planar beam fronts at this depth leading to more stable images. However, as shown in Figure 10 at other depths the partial image results in curved and broader beam fronts.

Figure 11 shows the complete imaging result for a single shot gather when focused Gaussian

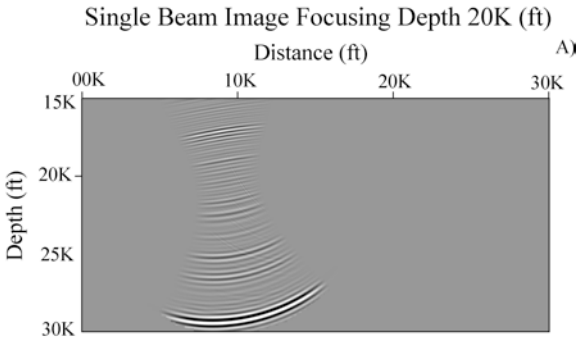

FIG. 10. *This shows the partial imaging result for a single Gaussian beam with the beam-waist shifted to about 20,000 ft in depth for a single shot gather from the Sigsbee2A dataset.*

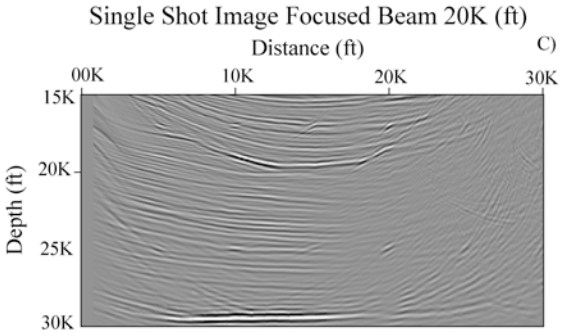

FIG. 11. *The Gaussian beam image using a complete single shot gather from the Sigsbee2A dataset with the shot location at 6325 ft using beams from all receiver positions launched at all angles each with the beam-waist shifted approximately 20,000 ft.*

beams are used with the beam-waists shifted approximately 20,000 ft from the receiver aperture. The shot location is at 6325 ft from the left edge of the model. Although only one of the 500 shots available in the Sigsbee2A dataset is used, the single shot image using focused Gaussian beams shows a number of the subsurface features for this part of the Sigsbee2A reflectivity model. Even though the beam-waists are specified for a depth of about 20,000 ft, the focused beam formulation still properly accounts for the variable curvature and beam widths at all depths of the image. When using other focusing depths, or with beam-waists at the surface, the simple shot images are all very similar to that shown in Figure 11. The advantage of using the focused beams is that for a target structure at a specific depth, fewer beams will be required to form a stable image. The results shown here are again for a smooth part of the Sigsbee2A background model well away from the salt dome structure. In a more complicated part of the model, focused beams could be designed to compensate for the focusing effects of the background model, in addition to minimizing the number of beams required for imaging. However, this needs to be further explored in future work.

4. Conclusions. The application of focused Gaussian beams has been investigated for seismic imaging. The shifting of the beam-waists away from the source and receiver aperture adds flexibility to Gaussian beam algorithms allowing for the narrowest portions of the beams to occur at the depth of a specific target structure. This minimizes the number of beams required to form an image at this target depth. Also, at the beam-waists the beam fronts are planar leading to more stable beam summations for imaging. To match with the surface data, a quadratic phase correction is required for the local slant-stacks of the data. Using the same local slant stacks of the data for the different imaging depths, only a single focusing depth can be specified. Imaging using focused Gaussian

beams was tested using a single shot gather for a model with 5 scatterers at different depths. The approach was then tested for a single shot gather from the Sigsbee2A model. In all cases, the beams can be focused to a particular target depth, but proper imaging still results for other depths as well.

Acknowledgments. This work was supported in part by the National Science Foundation and partly by the members of the Geo-Mathematical Imaging Group (GMIG) at Purdue University.

REFERENCES

[1] Babich, V.M and M.M. Popov (1989) *Gaussian summation method (Review)*, Izvestiya Vysshikh Uchebnykh Zavedenii, Radiofizika 32, 1447-1466 (Translated in Radiophysics and Quantum Electronics 32, 1063-1081, 1990).

[2] Bleistein, N. (2007) *Mathematics of modeling, migration and inversion with Gaussian beams*, Lecture Notes (online at http://www.cwp.mines.edu/ norm/).

[3] Cerveny, V. (1985a) *Gaussian beam synthetic seismograms*, J. Geophys., 58, 44-72.

[4] Cerveny, V. (1985b) *The applications of ray tracing to the numerical modeling of seismic wave fields in complex structures*, in Seismic Shear Waves (ed. G. Dohr) Geophysical Press, London, pp. 1-124.

[5] Cerveny, V. (2000) *Seismic Ray Theory*, Cambridge University Press.

[6] Cerveny, V., L. Klimes and I. Psencík (2007) *Seismic ray method: some recent developments*, Advances in Geophysics, 48, 1-128.

[7] Cerveny, V., M.M. Popov and I. Psencík (1982) *Computation of wavefields in inhomogeneous media – Gaussian beam approach*, Geophys. J.R. Astr. Soc., 70, 109-128.

[8] Feichtinger, H.G. and T. Strohmer (Eds.) (1998) *Gabor Analysis and Algorithms: Theory and Applications*, Birkhauser.

[9] Hale, D. (1992) *Migration by the Kirchhoff, slant stack and Gaussian beam methods*, CWD-121, Center for Wave Phenomena, Colorado School of Mines, Golden, CO.

[10] Hill, N. R. (1990) *Gaussian beam migration*, Geophysics, 55, 1416-1428.

[11] Hill, N. R. (2001) *Prestack Gaussian beam depth migration*, Geophysics, 66, 1240-1250.

[12] Lugara, D., C. Letrou A, Shlivinski, E. Heyman and A. Boag (2003) *Frame-based Gaussian beam summation method: Theory and applications*, Radio Science, Vol. 38, No. 2, 8026.

[13] Nowack, R.L. (2003) *Calculation of synthetic seismograms with Gaussian Beams*, Pure and Applied Geophys., 160, 487-507.

[14] Nowack, R.L. and K. Aki (1984) *The two-dimensional Gaussian beam synthetic method: testing and application*, J. Geophys. Res., 89, 7797-7819.

[15] Popov, M. M. (1982) *A new method of computation of wave fields using Gaussian beams*, Wave Motion, 4, 85-97.

[16] Popov, M. M. (2002) *Ray Theory and Gaussian beam method for geophysicists*, Lecture notes University of Bahia, Salavdor Brazil, 172 pp.

[17] Protasov, M.I. and V.A. Cheverda (2005) *True amplitude Gaussian beam imaging*, Proceedings of the International Seminar "Days on Diffraction – 2005", June 28-July 1 2005, St. Petersburg, Russia, pp. 225-234.

[18] Protasov, M.I. and V.A. Cheverda (2006) *True-amplitude seismic imaging*, Doklady Earth Sciences, Vol. 407A, 441-445.